Synchrotron x-ray scattering study of thin epitaxial Pr_2O_3 films on Si(001)

Xiangxin Guo,[a] Wolfgang Braun,[b] Bernd Jenichen, Vladimir M. Kaganer, Brad P. Tinkham, Achim Trampert, and Klaus H. Ploog
Paul-Drude-Institut für Festkörperelektronik, Hausvogteiplatz 5-7, D-10117 Berlin, Germany

(Received 7 February 2006; accepted 28 April 2006; published online 31 July 2006)

We investigate the structural and interfacial properties of thin Pr_2O_3 films on Si(001) substrates grown by molecular beam epitaxy using synchrotron grazing incidence x-ray diffraction and reflectivity measurements in ultrahigh vacuum. The epitaxial films consist of two orthogonal [101]-oriented cubic domains, with equal proportion. The average in-plane domain sizes are larger than the film thickness. Scans along crystal truncation rods confirm the cubic Mn_2O_3 structure of the epitaxial layer. A small amount of hexagonal Pr_2O_3 is found in thin films. Its fraction increases with increasing layer thickness indicating that it is not confined to the interface. Reflectivity measurements reveal an additional layer at the Pr_2O_3/Si(001) interface, which is extended by *in situ* annealing. Transmission electron microscopy of the samples confirms the structural properties of the films found by the x-ray measurements and shows that the interfacial layers are nonuniform with a coexistence of crystalline and amorphous regions. © *2006 American Institute of Physics*.
[DOI: 10.1063/1.2216421]

I. INTRODUCTION

Heteroepitaxial growth of high-κ (high dielectric constant) oxides on Si is of great importance for future gate dielectrics in complementary metal-oxide semiconductor (CMOS) technology.[1–8] The control of the film structure and the interfaces is a crucial issue in order to take advantage of the full potential of the high-κ oxides as well as the Si substrate underneath. Because of the pronounced chemical and structural differences between the crystalline oxide and the Si(001) substrate, this system is also an interesting object for fundamental studies of heteroepitaxy.[9–13]

Initial studies indicated crystalline Pr_2O_3 grown on Si(001) to be a promising candidate for scaled gate insulators.[14,15] The Pr_2O_3 was found to grow as [101]-oriented single crystal domains, with two orthogonal in-plane orientations. An improvement of the interface properties is highly desirable. Thermodynamic considerations predict the binary oxide Pr_2O_3 to be stable on silicon.[16] Two different phases have been reported for epitaxial Pr_2O_3, a cubic phase with a lattice constant of 11.152 Å and a hexagonal phase with $a=3.857$ Å and $c=6.016$ Å.[17,18] Studies of bulk Pr_2O_3 indicate that only the hexagonal phase is stable above 550 °C and both the hexagonal and the cubic phases can exist below 500 °C under standard conditions.[17] So far, Pr_2O_3 in the cubic Mn_2O_3 structure has been reported only for epitaxial films.[6,13] A unit cell of cubic Pr_2O_3 contains 32 metal atoms and 48 oxygen atoms arranged in a double-edge fluorite structure with one-fourth of the oxygen sites vacant and regularly ordered.[17] Clean Si(001) surfaces exhibit a two-domain (2×1)-reconstructed surface when the miscut is smaller than 2°.[19,20] The Si dimer rows on neighboring terraces are perpendicular to each other giving rise to the two different in-plane orientations of Pr_2O_3.

Grazing incidence x-ray diffraction (GIXRD) of synchrotron radiation is a versatile tool for the investigation of thin layers. The epitaxial relationship between the film and the substrate, the content of different phases in the layer, their island and domain sizes, and the lattice distortions can be obtained with a tunable penetration depth. In addition GIXRD provides a high sensitivity to other crystalline phases.

X-ray reflectivity (XRR) probes the layer thickness, the interface roughness, and interdiffusion at the interface. A density profile perpendicular to the sample surface can be obtained. Both methods (GIXRD and XRR) average over several mm^2 and give quantitatively relevant results.

In the present work, we apply these x-ray scattering methods in ultrahigh vacuum (UHV) for the characterization of the structural properties of crystalline Pr_2O_3 films on Si(001) substrates. We demonstrate the potential of these methods for the assessment of very thin high-κ dielectric films in terms of microstructure and the *in situ* detection of interfacial layers. For selected samples the results are compared to those of *ex situ* transmission electron microscopy (TEM).

II. EXPERIMENT

The Si(001) substrates were cleaned chemically by the RCA method[21,22] followed by a diluted hydrofluoric (HF) dip and a rinse in high-purity de-ionized water. After being loaded into the vacuum system, the substrates were outgassed at 150 and 330 °C in the load lock and the intermediate chambers, respectively. In the growth chamber, the hydrogen was desorbed while monitoring the reconstruction by

[a]Present address: ESRF, Grenoble, France; electronic mail: guo@esrf.fr
[b]Author to whom correspondence should be addressed; electronic mail: braun@pdi-berline.de

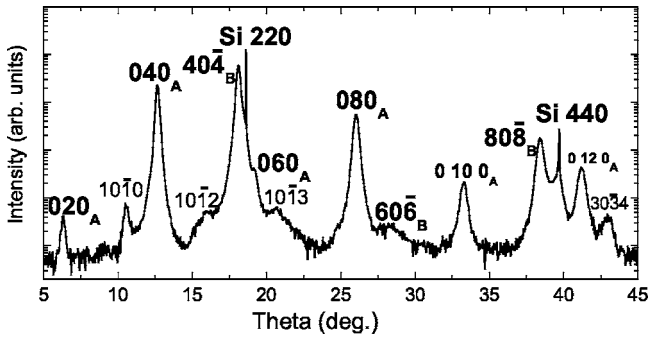

FIG. 1. In-plane GIXRD scan along Si [110] for a 14 nm thick Pr_2O_3 film grown at 600 °C. All substrate and oxide reflections are indexed in terms of their bulk lattices. The two kinds of domains of cubic Pr_2O_3 are labeled A and B. The directions [010] of domain A and $[10\bar{1}]$ of domain B are parallel to the Si[110] direction. Some weak reflections are due to hexagonal Pr_2O_3.

reflection high-energy electron diffraction (RHEED). A two-domain (2×1)-reconstructed Si surface was observed after hydrogen desorption.

Thin Pr_2O_3 films were grown on on-axis Si(001) substrates by electron beam evaporation of sintered ceramic Pr_2O_3 source targets under RHEED control in a multichamber UHV system. The growth temperature measured by a thermocouple near the backside of the sample was 600 °C, and the growth rate was 3 Å/min. During deposition, the UHV pressure was 2×10^{-9} mbar measured by an ion gauge near the substrate. Quadrupole mass spectrometry indicated both 16 and 32 mass peaks from oxygen in the growth chamber as the target material was partly dissociated.

After growth, the samples were transferred via an UHV shuttle from the growth molecular beam epitaxy (MBE) system to the measurement chamber mounted on a six-circle x-ray diffractometer.[23] The x-ray measurements were performed at the wiggler beam line U125/2 KMC at the storage ring BESSY (Berlin, Germany) using a double crystal Si(111) monochromator. An x-ray wavelength of 1.224 Å was used in the experiment. The acceptance angle of the detector was 0.1° both parallel and perpendicular to the surface.

After the measurements the films were capped with Al at about 100 °C in order to prevent reactions with air. The films were taken out of UHV and investigated by TEM and conventional high-resolution x-ray diffraction (HRXRD). Electrical measurements were performed as described in Ref. 24.

III. RESULTS AND DISCUSSION

A. In-plane GIXRD scans

Figure 1 shows a wide-range in-plane GIXRD (ω-2Θ) scan of a thin Pr_2O_3 film on Si(0 0 1). This scan is performed along the Si[110] direction. The film thickness is about 14 nm, measured by x-ray reflectivity in the same UHV chamber. All the substrate and oxide reflections are indexed in terms of their bulk lattices.

The film consists of two types of domains (A and B) in the cubic Mn_2O_3 structure with two orthogonal in-plane orientations. The directions [0 1 0] of domain A and $[1\ 0\ \bar{1}]$ of domain B are parallel to Si [1 1 0]. Both domains have the (1 0 1) plane parallel to the Si(0 0 1) surface, which is consistent with the results of conventional ω-2Θ XRD scans. The in-plane lattice parameters of both domains can be calculated from the Pr_2O_3 020_A, 040_A, 080_A, 0100_A, 0120_A, $40\,\bar{4}_B$, and $80\,\bar{8}_B$ reflections taking the Si reflections as a reference. The resulting lattice constants are 11.04 Å along the [0 1 0] direction of domain A and 7.81 Å along the $[1\ 0\ \bar{1}]$ direction of domain B. Compared to the lattice constant of bulk Pr_2O_3 (Ref. 17) the measured in-plane lattice parameters deviate less than 1%. We measured a perpendicular scan along the Si Si$[1\ \bar{1}\ 0]$ direction as well. The resulting curve exactly coincides with that of the scan along Si [1 1 0]. This means that the two domains grow in an equal proportion and have the same in-plane lattice constants. Rocking scans for the observed in-plane reflections reveal a typical in-plane mosaic spread of 1.5°.

Several weak reflections observed in the film can be assigned to the hexagonal phase of Pr_2O_3. This hexagonal Pr_2O_3 is not observed during growth by *in situ* RHEED. As confirmed by x-ray measurements with different penetration depths, some fraction of the hexagonal phase exists throughout the entire film thickness of 14 nm. Comparing with other samples we find that the quantity of hexagonal Pr_2O_3 depends on the film thickness. For films thicker than 18 nm, the hexagonal reflection intensities become much stronger. Probably some hexagonal Pr_2O_3 grains already nucleate at the Pr_2O_3/Si interface and their amount grows with increasing layer thickness. The cubic phase of Pr_2O_3 is stabilized by the square surface symmetry of the substrate during the very first phase of the epitaxial growth.[24]

In Fig. 1, several diffraction orders of the two cubic domains are present. These reflections allow us to estimate the average domain sizes together with the strain in the domains from Williamson-Hall (WH) plots.[26–29] The peaks in the $\omega/2\Theta$ scans are fitted well by Gaussian functions. They are broadened by the finite size of the diffracting domains as well as by inhomogeneous deformations inside the domains. The integrated width of the physically broadened profile β_f of the sample consists of the size and strain components β_s and β_D. The size component β_s does not depend on the diffraction angle. The strain component β_D increases linearly with the order of the reflection. For Gaussian peak profiles one assumes[28]

$$(\beta_f^*)^2 = (\beta_S^*)^2 + (\beta_D^*)^2 = (\beta_S^*)^2 + (2ed^*)^2, \tag{1}$$

where

$$e = \beta_D^*/2d^* = \Delta d/d \tag{2}$$

is the strain variation within the domains, $|d^*| = 1/d = 2\sin(\theta)/\lambda$ is the absolute value of the reciprocal lattice vector $\beta_f^* = \beta_f \cos(\theta)/\lambda$, θ is the Bragg angle, and λ is the wavelength. The width of the physically broadened profile β_f can be obtained from

$$(\beta_f)^2 = (\beta_h)^2 - (\beta_g)^2, \tag{3}$$

where β_h is the integral width of the measured curve calculated as the integrated intensity divided by the peak intensity of the corresponding maximum. The values of β_h are in the

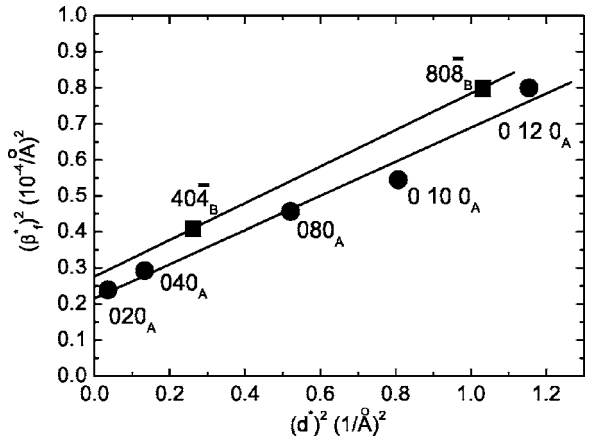

FIG. 2. Williamson-Hall plot in reciprocal lattice representation for the Gaussian line profiles. $|d^*|=1/d=2\sin(\theta)/\lambda$ is the length of the reciprocal lattice vector and $\beta_f^*=\beta_f\cos(\theta)/\lambda$, where β_f is the integral width of the physically broadened profile, θ is the Bragg, angle, and λ is the wavelength.

range of 0.4°–0.9°. β_g is the width of the apparatus function, which is approximated by a Gaussian of 0.1° integral width.[29] The WH plots, i.e., $(\beta_f^*)^2$ over $(d^*)^2$, for both types of domains are shown in Fig. 2.

The intersection with the ordinate leads to β_s^*, which gives the lateral domain size

$$l = 1/\beta_S^*. \tag{4}$$

We obtain 22 nm for domain A and 19 nm for domain B along the Si[1 1 0] direction. The strain variations within the domains e obtained from the slope of the WH plot are 0.35% for domain A and 0.34% for domain B.

B. Out-of-plane scans along crystal truncation rods

Figures 3(a) and 3(b) present out-of-plane scans along the 080_A and $80\bar{8}_B$ rods for domains A and B, respectively. From the peak positions of different order reflections, the out-of-plane lattice constant can be calculated. The resulting value along the [1 0 1] direction is close to 8.03 Å for both domains. Compared to the lattice constant of bulk Pr_2O_3, both domains are expanded by about 0.3% along. [1 0 1] Comparing Fig. 3(a) with 3(b), we note that the forbidden reflections 9 0 $\bar{7}_B$ and 11 0 $\bar{5}_B$ (i.e., $8+L\ 0\ \bar{8}+L$ reflections with $L=1$ and 3) are indeed absent in the scan along the 80 $\bar{8}_B$ rod. This confirms that the domains grow in the cubic Mn_2O_3 structure.

Out-of-plane $\omega/2\Theta$ scans in conventional high-resolution x-ray diffraction confirm that the lattice expansion is below 1% in the direction perpendicular to the interface.[30]

C. Reflectivity

Reflectivity measurements as well as the GIXRD measurements were carried out in UHV before and after annealing the samples. The annealing took place at 700 °C for 10 min in the UHV measurement chamber. In-plane GIXRD shows no obvious change of the film structure after annealing. However, the reflectivity data show a significant change of the interference fringes. As shown in Fig. 4, the oscillations notably vary in the range of incidence angles larger

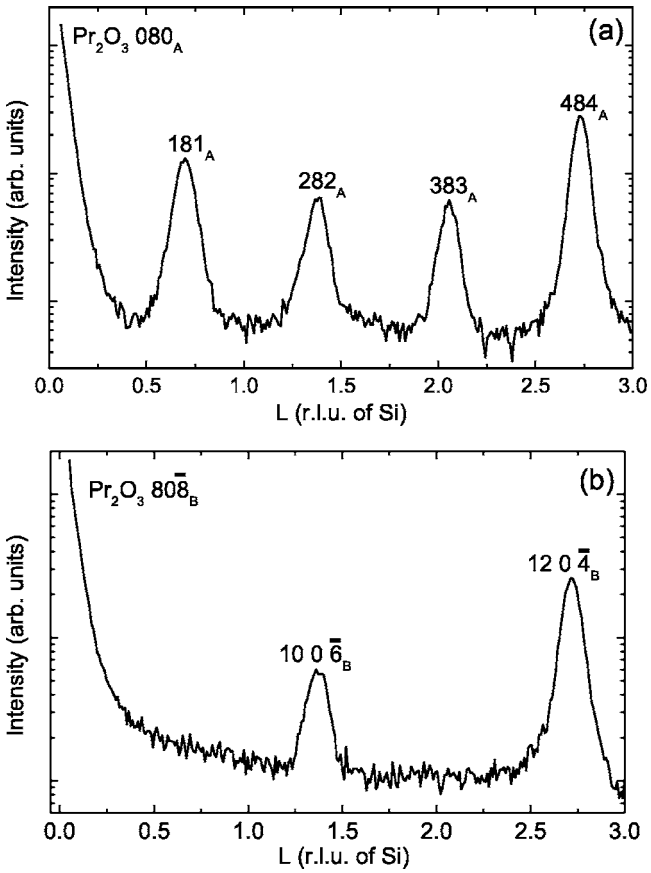

FIG. 3. GIXRD scans along the crystal truncation rods of (a) 080_A and (b) $80\bar{8}_B$ both terminating on the same in-plane direction. In the latter case, the forbidden reflections 90 $\bar{7}_B$ and 11 0 $\bar{5}_B$ (i.e., $8+L\ 0\ \bar{8}+L$ reflections with $L=1$ and 3) are absent. This confirms the cubic Mn_2O_3 structure of the layer.

than 1°. In the figure, the open circles represent the measured data points and the solid lines are fits using a modified Parratt algorithm.[31–33] The inset shows the density profiles obtained from the simulations. The layer parameters resulting from the fits to the experimental data are listed in Table I.

For the as-grown sample, a good fit to the experimental data is obtained by introducing a 1.7 nm thick interfacial

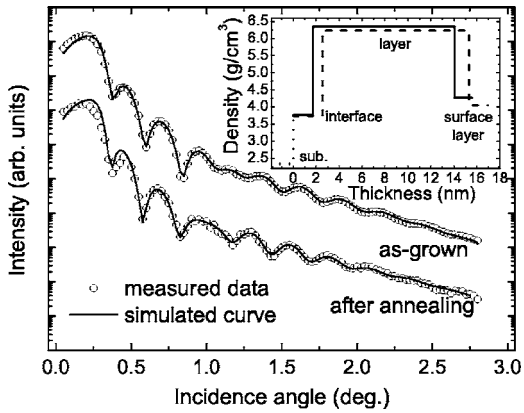

FIG. 4. Reflectivity data for a Pr_2O_3/Si layer as grown and after annealing at 700 °C for 10 min in the UHV measurement chamber. The open circles represent the measured data points and the solid lines are fits to the experimental data. Density profiles for the simulations are displayed in the inset. The full line shows the profile for the as-grown sample and the dashed line corresponds to the profile of the annealed sample. The layer parameters resulting from the fits to the experimental data are listed in Table I.

TABLE I. Layer parameters resulting from the fit to the measured data for the as-grown and the annealed sample.

Layer	Layer description	Density (g/cm^3) as grown/ annealed	Thickness (nm) as grown/ annealed	Roughness (nm) as grown/ annealed
1	Si–O–Pr	3.76/3.74	1.7/2.6	0.3/0.3
2	Pr_2O_3	6.35/6.23	12.3/12.8	0.7/0.7
3	Surface Pr_2O_3	4.27/4.04	1.5/1.7	0.9/1.0

layer between the Si substrate and the Pr_2O_3 film and a 1.5 nm thick surface Pr_2O_3 layer with a reduced density (see Table I, and inset in Fig. 4, full line). The resulting Pr_2O_3 film thickness is 12.3 nm. The interfacial layer has a density in between Si and cubic Pr_2O_3. Presumably, it is an amorphous interface layer as reported in Ref. 34. Since the sample stays in UHV all the time, the density deviation near the surface of the Pr_2O_3 layer should be attributed to a change of surface roughness. A rough interface and a rough upper surface from the faceting of individual domains were indeed observed by scanning TEM in crystalline Gd_2O_3 films grown on a Si(001) substrate.[3]

For the characterization of the sample after annealing, the experimental data are fitted using the same method as for the as-grown sample. The fit yields a 2.6 nm thick interfacial layer, a 12.8 nm thick film, and a 1.7 nm thick surface Pr_2O_3 layer (see Table I, and inset in Fig. 4, dashed line). The interfacial layer is obviously extended by the annealing. While the thicknesses of the other layers also increase after annealing, their densities decrease. An expected grading between the substrate and the interface layer is introduced as a roughness.[32] The thickness of this grading is 1.3 nm before annealing and increases to 1.4 nm after annealing. According to the previous work,[25] a pronounced Si segregation occurs during growth at 600 °C, as well as a Si diffusion from the substrate into the film during postdeposition annealing. This Si diffusion has the effect to bring more Si atoms to the interface and drive more Si from the interface to the film, which is most probably responsible for the variations of the layer properties of the annealed sample. There is a relatively large decrease of the density of the upper surface Pr_2O_3 layer together with an increase of the thickness. Possible contributions to this decrease of density may come from the Si diffusion and a possible roughening of the surface.

D. Results of the *ex situ* investigations

After growth and thermal treatment, the films were capped with Al layers, the samples were taken out of UHV, and some of them were investigated by TEM and HRXRD. HRXRD measurements show diffraction peaks from the cubic phase[17] of the Pr_2O_3 layer. The measured position of the Pr_2O_3 (1 0 1) peak with respect to the Si (0 0 4) substrate reflection allows to conclude that the tetragonal deformation of the film is less than 1%. As shown in Fig. 5(a) by TEM, the film is continuous and uniform on the microscopic scale. The upper surface of the Pr_2O_3 is rather rough. The electron diffraction pattern of the area in the bright square in Fig. 5(a)

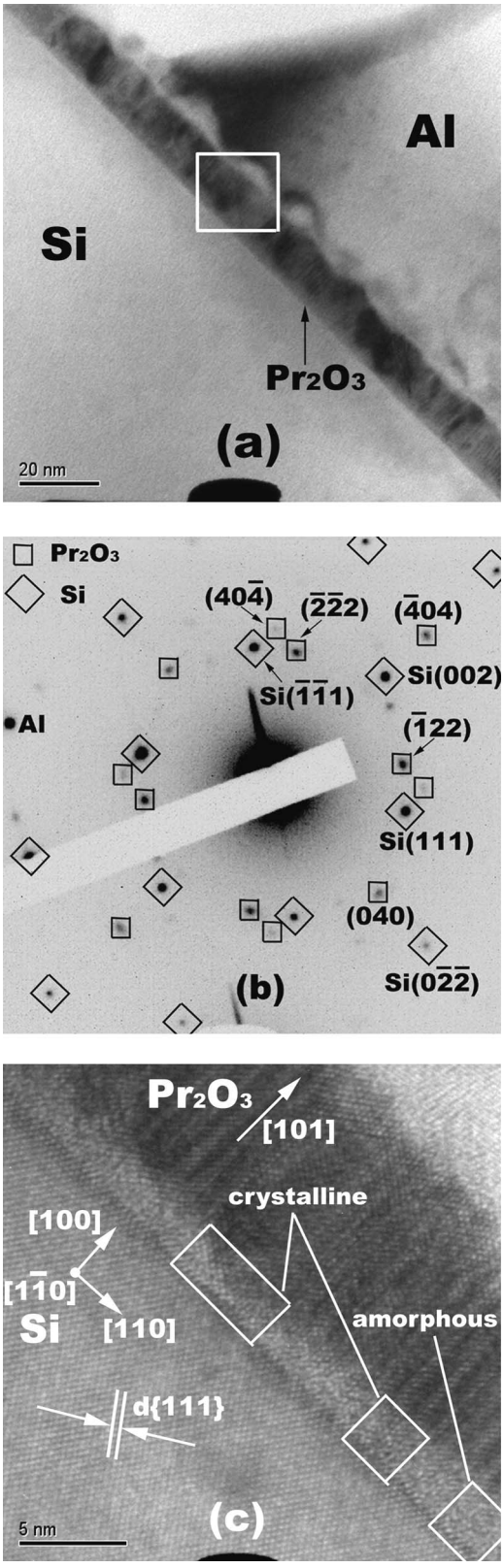

FIG. 5. (a) Cross-sectional TEM image of Pr_2O_3 film capped with Al after a 10 min *in situ* anneal at 700 °C. The film is continuous and uniform. The bright square indicates the area selected for (b) electron diffraction and (c) high-resolution TEM measurements. The diffraction pattern confirms two orthogonal domains with $Pr_2O_3(101)\|Si(001)$ and $Pr_2O_3[010]$ or $[10\bar{1}]\|Si[110]$ Hexagonal Pr_2O_3 is here below the detection limit. The high-resolution image is obtained with the electron beam parallel to the $Si[1\bar{1}0]$ direction. It shows a rough Si substrate surface and a nonuniform interfacial layer with a mixture of crystalline and amorphous regions.

is shown in Fig. 5(b). The diffraction signals of the two orthogonal domains with $Pr_2O_3(101)\|Si(0\ 0\ 1)$ and Pr_2O_3 $[0\ 1\ 0]$ or $[1\ 0\ \bar{1}]\|Si[110]$ are superimposed. No hexagonal Pr_2O_3 is detected in this area.

The high-resolution TEM image, Fig. 5(c), clearly shows a nonuniform interfacial layer of a thickness ranging from 0.5 to 2.5 nm. This interfacial layer is a mixture of crystalline and amorphous regions. The crystalline parts exhibit a structure similar to the epitaxial film. These findings correlate well with the above results obtained from the GIXRD scans. Electrical measurements performed at one of the annealed samples yield a dielectric constant κ of 15, still a factor of 2 lower than the value in Ref. 24 The corresponding leakage current density of this sample is 10^{-6} A/cm^2 at a gate voltage of 1 V which is higher than the values obtained in Ref. 24 So the electrical properties of our samples still need further improvement. We think that the high-κ properties of our Pr_2O_3 films are compromised by interface layers.

IV. SUMMARY

The film structure and interfacial properties of MBE-grown Pr_2O_3 thin films on Si(001) substrates have been investigated *in situ* in UHV by synchrotron-radiation grazing incidence x-ray diffraction and reflectivity. In addition, *ex situ* TEM and conventional high-resolution x-ray diffraction investigations were performed after capping. Our films contain two types of orthogonal [101]-oriented domains exhibiting the cubic Mn_2O_3 structure; the [010] directions of the one and $[10\bar{1}]$ of the other are parallel to Si[110]. The average in-plane domain sizes are larger than the film thickness. Only a very small amount of hexagonal Pr_2O_3 is found for thin layers with thicknesses below 10 nm. Its fraction increases with growing thickness. This implies that the cubic phase is stabilized near the interface. Reflectivity measurements reveal that as-grown films contain an additional layer at the Pr_2O_3/Si(001) interface. *In situ* annealing in UHV leads to the extension of this interface layer. The TEM clearly detects such nonuniform interfacial layers in the samples. It also reveals the coexistence of crystalline and amorphous phases at the interface. The interfacial layers compromise the electrical properties. They have to be avoided in the future, possibly by the choice of another more stable gate material and/or by a fine tuning of the growth conditions under *in situ* control.

ACKNOWLEDGMENTS

The authors are indebted to M. Takahasi and D. K. Satapathy for help with the x-ray experiment and H. Gottlob (AMO GmbH) for the electrical measurements. This work is financed by the German Federal Ministry of Education and Research in the framework of the project KrisMOS (Grant No. 01M3142D).

[1] R. A. McKee, F. J. Walker, and M. F. Chrisholm, Science **293**, 468 (2001).
[2] H. Mori and H. Ishiwara, J. Appl. Phys. **30**, 1415 (1991).
[3] J. Kwo *et al.*, J. Appl. Phys. **89**, 3920 (2001).
[4] R. Droopad *et al.*, J. Cryst. Growth **251**, 638 (2003).
[5] S. Guha, E. Cartier, M. A. Gribelyuk, N. A. Bojarczuk, and M. C. Copel, Appl. Phys. Lett. **77**, 2710 (2000).
[6] H. J. Osten, J. P. Liu, E. Bugiel, H. J. Müssig, and P. Zaumseil, J. Cryst. Growth **235**, 229 (2002).
[7] A. Dimoulas, G. Vellianitis, A. Travlos, V. Ioannou-Sougleridis, and A. G. Nassiopoulou, J. Appl. Phys. **92**, 426 (2002).
[8] S. C. Choi, M. H. Cho, S. W. Whangbo, C. N. Whang, S. B. Kang, S. I. Lee, and M. Y. Lee, Appl. Phys. Lett. **71**, 903 (1997).
[9] R. A. McKee, F. J. Walker, and M. F. Chisholm, Phys. Rev. Lett. **81**, 3014 (1998).
[10] C. J. Först, C. R. Ashman, K. Schwarz, and E. B. Peter, Nature (London) **427**, 53 (2004).
[11] J. Lettieri, J. H. Haeni, and D. G. Schlom, J. Vac. Sci. Technol. A **20**, 1332 (2002).
[12] H.-J. Müssig, J. Dabrowski, K. Ignatovich, J. P. Liu, V. Zavodinsky, and H. J. Osten, Surf. Sci. **504**, 159 (2002).
[13] T. Schroeder, T.-L. Lee, J. Zegenhagen, C. Wenger, P. Zaumseil, and H.-J. Müssig, Appl. Phys. Lett. **85**, 1229 (2004).
[14] H. J. Osten, E. Bugiel, and A. Fissel, Solid-State Electron. **47**, 2161 (2003).
[15] H. J. Osten, J. P. Liu, E. Bugiel, H. J. Müssig, and P. Zaumseil, Mater. Sci. Eng., B **87**, 298 (2001); P. Zaumseil and T. Schroeder, J. Phys. D **38**, A179 (2005).
[16] D. G. Schlom and J. H. Haeni, in *Alternative Gate Dielectrics for Microelectronics*, edited by G. Wilk and R. M. Wallace, special issue of MRS Bull. **27**, 198 (2002).
[17] G.-Y. Adachi and N. Imanaka, Chem. Rev. (Washington, D.C.) **98**, 1479 (1998).
[18] O. Greis, R. Ziel, B. Breidenstein, A. Haase, and T. Petzel, J. Alloys Compd. **216**, 255 (1994).
[19] J. Dabrowski and H.-J. Müssig, *Silicon Surfaces and Formation of Interfaces* (World Scientific, Singapore, 2000).
[20] B. Voigtländer, Surf. Sci. Rep. **43**, 127 (2001).
[21] W. Kern and D. A. Puotinen, RCA Rev. **31**, 187 (1970).
[22] R. C. Henderson, J. Electrochem. Soc. **119**, 772 (1972).
[23] B. Jenichen, W. Braun, V. M. Kaganer, A. G. Shtukenburg, L. Däweritz, C. G. Schulz, and K. H. Ploog, Rev. Sci. Instrum. **74**, 1267 (2003).
[24] A. Fissel, H. J. Osten, and G. Bugiel, J. Vac. Sci. Technol. B **21**, 1765 (2003).
[25] G. Lippert, J. Dabrowski, V. Melnik, R. Sorge, Ch. Wenger, P. Zaumseil, and H.-J. Müssig, Appl. Phys. Lett. **86**, 042902 (2005).
[26] B. E. Warren, *X-ray Diffraction* (Addison-Wesley, Reading, MA, 1969).
[27] H. P. Klug and L. E. Alexander, *X-ray Diffraction Procedures* (Wiley, New York, 1974).
[28] J. I. Langford, in *Industrial Applications of X-ray Diffraction*, edited by F. H. Chung and D. K. Smith (Dekker, New York, 2000), p. 751.
[29] B. Jenichen, D. Satapathy, W. Braun, L. Däweritz, and K. H. Ploog, J. Appl. Phys. **96**, 6103 (2004).
[30] J. Hornstra and W. J. Bartels, J. Cryst. Growth **44**, 513 (1978).
[31] L. G. Parratt, Phys. Rev. **95**, 359 (1954).
[32] L. Névot and P. Croce, Rev. Phys. Appl. **15**, 761 (1980).
[33] Program REFLECTIVITY supplied by PANalytical.
[34] D. Schmeißer, H.-J. Müssig, and J. Dabrowski, Appl. Phys. Lett. **85**, 88 (2004).